Laboratori Nazionali di Frascati

Submitted to Nucl. Instr. & Meth. in Physics Research

LNF-93/009 (P)
26 Febbraio 1993

S. Bartalucci, M. Serio, B. Spataro, M. Zobov, L. Palumbo:

BROAD-BAND MODEL IMPEDANCE FOR DAΦNE MAIN RINGS

PACS.: 29.27.Bd

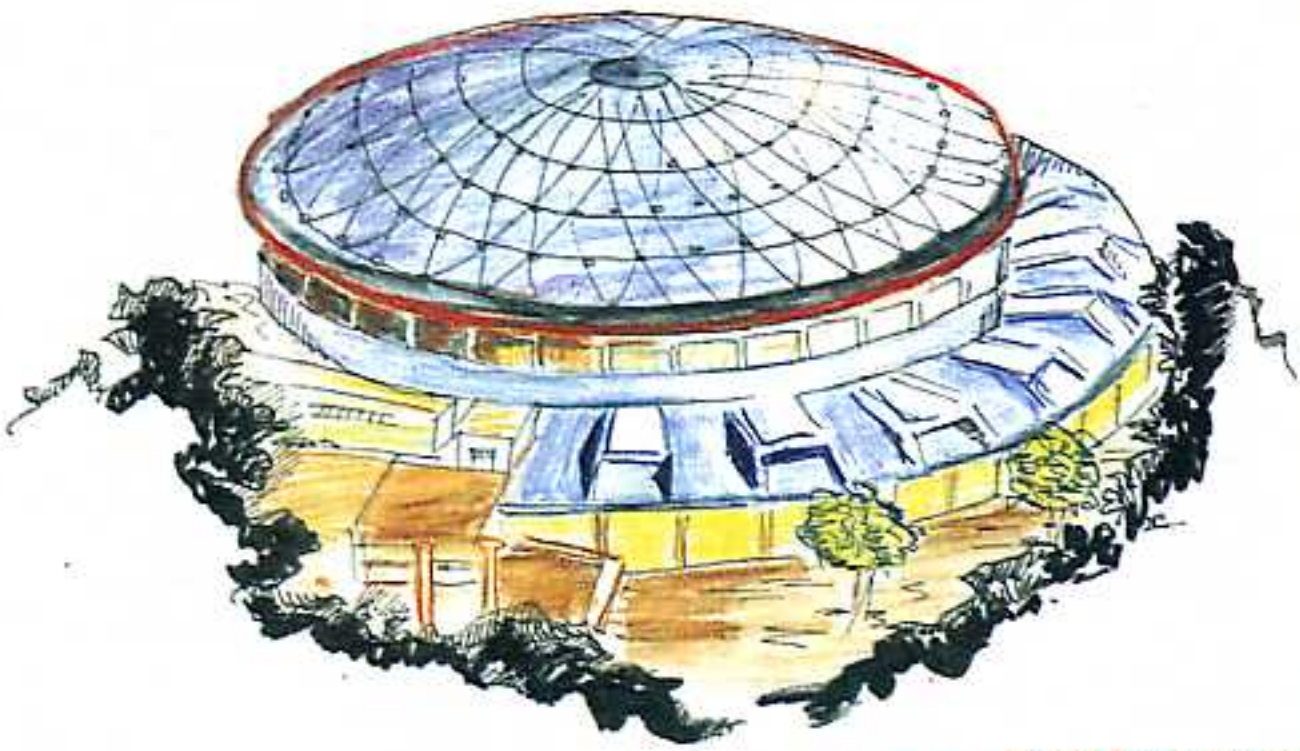

Servizio Documentazione
dei Laboratori Nazionali di Frascati
P.O. Box, 13 - 00044 Frascati (Italy)

INFN – Laboratori Nazionali di Frascati
Servizio Documentazione

LNF-93/009 (P)
26 Febbraio 1993

BROAD-BAND MODEL IMPEDANCE FOR DAΦNE MAIN RINGS

S. Bartalucci, M. Serio, B. Spataro, M. Zobov
INFN – Laboratori Nazionali di Frascati, P.O. Box 13, I – 00044 Frascati (Roma), Italy

L. Palumbo
Dip. Energia, Univ. La Sapienza, Via A. Scarpa 14, 00161 (Roma), Italy
and Laboratori Nazionali di Frascati dell'INFN, I – 00044 Frascati (Roma), Italy

ABSTRACT

A recently proposed model has been used to describe the broad–band impedance of the vacuum components of the DAΦNE storage rings. Numerical calculations of the loss factor and the wake potential in the time and frequency domain are in good agreement with the model predictions.

1. – INTRODUCTION

In order to investigate single bunch instability it is sufficient to consider short range wake potentials over the bunch length. This allows to replace the actual impedance, which can be a very complicated function of frequency, by a broad–band model impedance. The broad–band model impedance is simple and convenient in analytical calculations of stability limits.

The widely used broad–band resonator model of the impedance[1] is described by only three parameters: shunt impedance R, quality factor Q and angular resonant frequency ω_r. When the bunch length is long compared with the beam pipe radius, the number of parameters is reduced to one: the low frequency limit of the normalized longitudinal impedance $Z/n = R\omega_r/\omega_0$ (ω_0 is the revolution frequency and ω_r is close to the cutoff frequency of the lowest TM waveguide mode in the vacuum pipe). But the broad–band resonator model has its own limits for shorter bunches. For example, it fails to describe high frequency behavior of a cavity with attached tubes or a periodic array of cavities.

There is also another shortcoming of the broad–band resonator model. The usual procedure to get the parameters of the model is to fit numerical dependence of the longitudinal loss factor k_l on the RMS bunch length σ. But the loss factor is related only to the real part of the impedance and some information about the imaginary part can be lost (namely, the imaginary part is responsible for the potential–well bunch lengthening). Moreover, as numerical calculations show, good fitting of $k_l(\sigma)$ does not necessarily imply good fitting of the wake–functions, i.e. wake–functions corresponding to the broad–band resonator model could be rather different from those given by numerical codes.

Below we apply another recently proposed broad–band impedance model[2,3] which is described by expansion over $\sqrt{\omega}$. It seems to be more suitable than the usual broad–band resonator model to describe impedance generating elements of the DAΦNE main ring. We have found that it is enough to take only the four first terms in the expansion to get a satisfactory fit to both the longitudinal loss factor and the wake–functions of all vacuum chamber components simulated so far. The coefficients of the expansion are extracted from wake–functions or loss factors given by numerical codes TBCI or MAFIA[4, 5].

2. – BASIC FORMULAE

The broad–band impedance is described by the expansion over $\sqrt{\omega}$:

$$Z(\omega) = - i\omega L + R + (1 - i)\sqrt{\omega}B + \frac{1 + i}{\sqrt{\omega}}Z_c + \dots \qquad (1)$$

The coefficients L, R, B, Zc,..., are real. These coefficients can be extracted from wake–functions and loss factors given by TBCI and MAFIA codes.

The wake–functions and longitudinal loss factors which correspond to the impedance (1) are given by well–known expressions:

$$W(s) = \frac{1}{2\pi}\int_{-\infty}^{\infty} Z(\omega)\,\tilde{\lambda}(\omega)\,e^{-i\omega s/c}\,d\omega \qquad (2)$$

$$k_l(\sigma) = \frac{1}{2\pi}\int_{-\infty}^{\infty} Z(\omega)\left|\tilde{\lambda}(\omega)\right|^2 d\omega \qquad (3)$$

where $\tilde{\lambda}(\omega)$ is the Fourier transform of the bunch line density. For Gaussian density:

$$\tilde{\lambda}(\omega) = \exp\{-\frac{\omega^2\sigma^2}{2c^2}\} \qquad (4)$$

1. Let us consider a purely inductive impedance for all frequencies in the bunch spectrum:

$$Z(\omega) = -i\omega L, \quad \omega\sigma/c < 1 \qquad (5)$$

Then using the relation[6]:

$$\int_0^\infty dx\, x \exp\{-p^2 x^2\} \sin ax = \frac{a\sqrt{\pi}}{4 p^3} \exp\{ -\frac{a^3}{4 p^3} \} \tag{6}$$

formula (2) gives:

$$W(s) = -\frac{L c^2}{\sqrt{2\pi}\, \sigma^3} s \exp\{ -\frac{1}{2}\left(\frac{s}{\sigma}\right)^2 \} \tag{7}$$

This wake–function has a minimum (maximum) at $s = -\sigma(+\sigma)$:

$$W_{max} = - W_{min} = \frac{L c^2}{\sqrt{2\pi e}\, \sigma^2} \tag{8}$$

The wake–function (7) is typical of small discontinuities, such as shielded bellows and vacuum ports, slots, shallow cavities in flanges and so on. The plot of $-W(s)/|W|_{max}$ which is suitable to be compared with TBCI results is shown in Fig. 1.

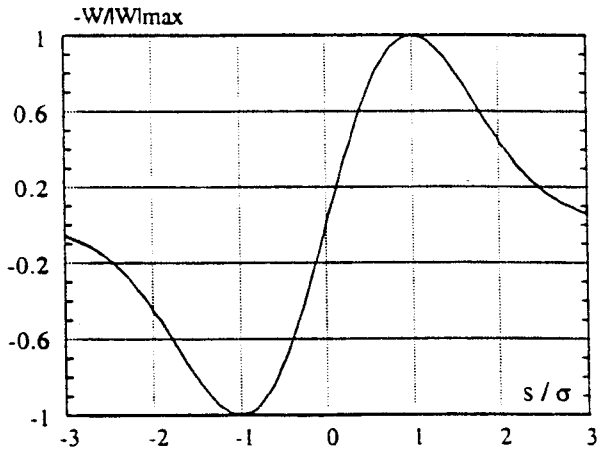

FIG. 1 – Normalized wake–function corresponding to the inductive impedance $Z(\omega) = -i\omega L$.

The longitudinal loss factor for the inductive impedance is equal to:

$$k_l = 0. \tag{9}$$

2. For a resistive impedance:

$$Z(\omega) = R, \ \omega\sigma/c < 1 \tag{10}$$

eqs. (2) and (3) correspondingly give:

$$W(s) = -\frac{R c}{\sqrt{2\pi}\, \sigma} \exp\{ -\frac{1}{2}\left(\frac{s}{\sigma}\right)^2 \} \tag{11}$$

$$k_1 = \frac{R\,c}{2\sqrt{\pi}\,\sigma} \tag{12}$$

To get eq.(11) we used the relation[6]:

$$\int_0^\infty dx\, \exp\{-\beta\, x^2\}\, \cos bx = \frac{1}{2}\sqrt{\frac{\pi}{\beta}}\, \exp\{-\frac{b^2}{4\beta}\} \tag{13}$$

The function given by eq. (11) has the same dependence on s as the charge density with a maximum at s = 0. $-W(s)/|W|_{max}$ is shown in Fig. 2.

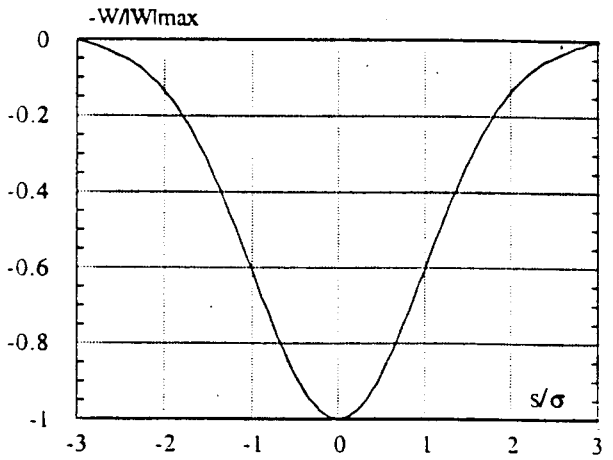

FIG. 2 – Normalized wake–function corresponding to the resistive impedance $Z(\omega) = R$.

3. Let us now consider the third term in eq.(1). It has the structure of the resistive wall impedance:

$$Z(\omega) = (1 - i)\, B\sqrt{\omega},\ \ \omega\sigma/c < 1 \tag{14}$$

To get the wake–function for the impedance we use a property (see for example Ref. 7):

$$\int_0^\infty d\omega\, \exp\{-a\,\omega^2 + i\omega y\}\sqrt{\omega} = \frac{\pi\, y\, \sqrt{|y|}}{4\, a\, \sqrt{8\, a}}[I_{-3/4} - I_{1/4} \pm i(I_{-1/4} - I_{3/4})]e^{-b} \tag{15}$$

for $\pm\, y > 0$. I_ν are the modified Bessel functions of argument $b = y^2/8a$.

And, finally:

$$W(s) = \frac{B\, c^{3/2}}{4\, \sigma^{3/2}}\left(\frac{|s|}{\sigma}\right)^{3/2}\left\{I_{-3/4}(b) - I_{1/4}(b) - I_{-1/4}(b) \pm I_{3/4}(b)\right\} e^{-b} \tag{16}$$

where $b = s^2/4\,\sigma^2$.

$\pm$ sign corresponds to positive and negative "s", respectively.

Fig. 3 shows the dependence $-W(s)/|W|_{max}$.

Using the definition (3) we get a simple formula for the longitudinal loss factor:

$$k_l = \frac{B}{\pi}\left(\frac{c}{\sigma}\right)^{3/2}\frac{\Gamma(3/4)}{2} \tag{17}$$

where $\Gamma(3/4)/2 = 0.6127...$

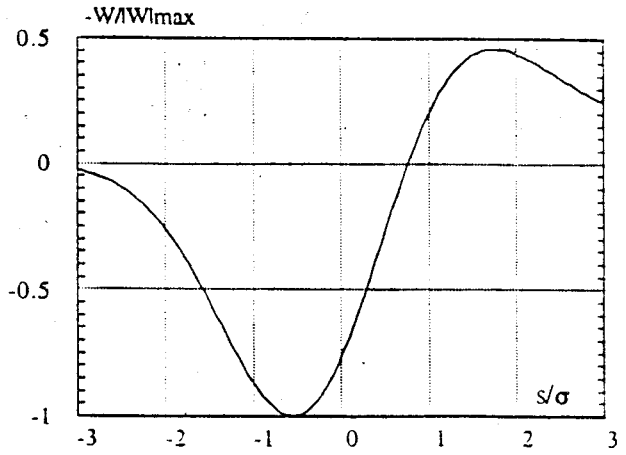

FIG. 3 – Normalized wake–function corresponding to the impedance $Z(\omega) = (1 - i)\, B\sqrt{\omega}$.

4. The last term in (1) has the same dependence on ω as the impedance of a cavity with attached tubes at high frequencies:

$$Z(\omega) = \frac{(1+i)\,Z_c}{\sqrt{\omega}}, \quad \omega\sigma/c < 1 \tag{18}$$

Taking into account that[6]:

$$\int_0^\infty \frac{d\omega}{\sqrt{\omega}} \exp\{-a\,\omega^2 + i\omega y\} = \frac{\pi\sqrt{|y|}}{\sqrt{8\,a}}(I_{-1/4}(b) \pm i\, I_{1/4}(b))e^{-b} \tag{19}$$

with $\pm y > 0$ and $b = y^2/8a$ and $a = \sigma^2/2\,c^2$ we get an expression for the wake–function:

$$W(s) = \frac{Z_c\, c^{1/2}}{2\,\sigma^{1/2}}\left(\frac{|s|}{\sigma}\right)^{1/2}\left\{I_{-1/4}(b) \pm I_{1/4}(b)\right\} e^{-b} \tag{20}$$

$\pm$ sign stands for positive and negative "s". The function $-W(s)/|W|_{max}$ is given in Fig. 4.

Using (2) we obtain the expression for the loss factor :

$$k_l = \frac{Z_c}{\pi}\left(\frac{c}{\sigma}\right)^{1/2}\frac{\Gamma(1/4)}{2} \tag{21}$$

with $\Gamma(1/4)/2 = 1.8128...$

The parameters L, R, B, Zc, of the broad–band impedance model are extracted from TBCI or MAFIA results by fitting the numerical function W(s) and kl(σ) to the analytical expressions (7)–(8), (11)–(12), (16)–(17), (20)–(21).

Below we apply this procedure for the impedance calculation of the DAΦNE main ring vacuum chamber elements[8].

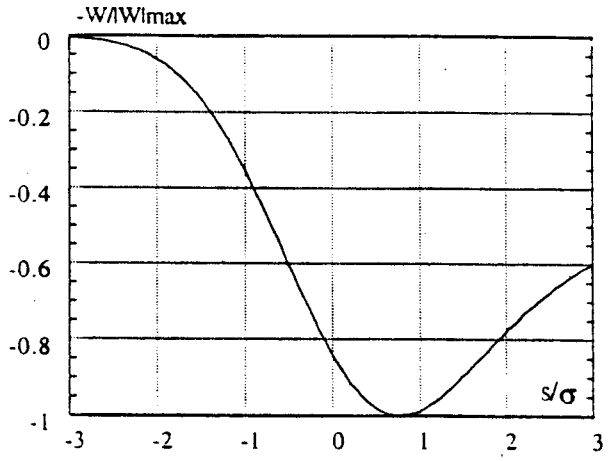

FIG. 4 – Normalized wake–function corresponding to the impedance $Z(\omega) = \frac{(1+i)\,Z_c}{\sqrt{\omega}}$.

3. – RF CAVITY

A low loss cavity has been proposed for DAΦNE main rings[8]. The main feature of the cavity is the presence of long tapers, which provide a smooth transition from the cell iris to the ring vacuum chamber (Fig. 5).

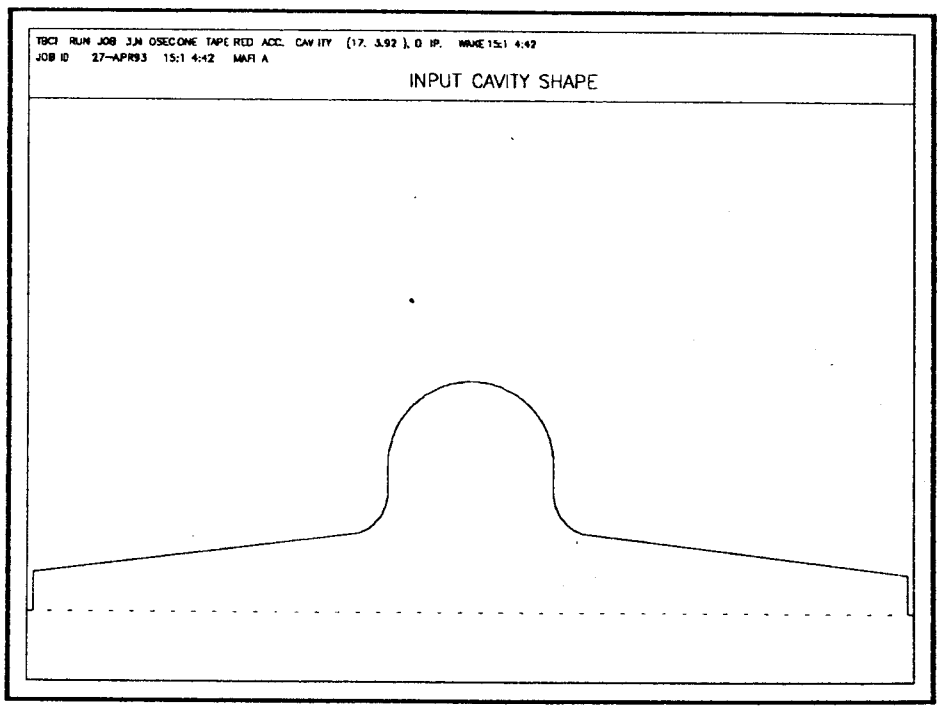

FIG. 5 – DAΦNE RF cavity shape.

We have estimated the longitudinal impedance of the cavity using two broad–band impedance models: the usual broad–band resonator model and the model given by expansion (1).

For the resonator broad–band model a fit of the computed dependence $k_l(\sigma)$ was used to extract the resonator parameters: shunt impedance R, quality factor Q and angular resonant frequency ω_r. Figure 6 shows the numerical dependence $k_l(\sigma)$ (open squares) and its fit, which corresponds to the broad–band resonator with $|Z/n|_0 = R\omega_r/\omega_0 = 0.614\ \Omega$, $\omega r = 3.58*10^9$ rad/sec and Q = 1 (full dots). The fit does not improve substantially by varying Q in the range from 0.5 to 1.

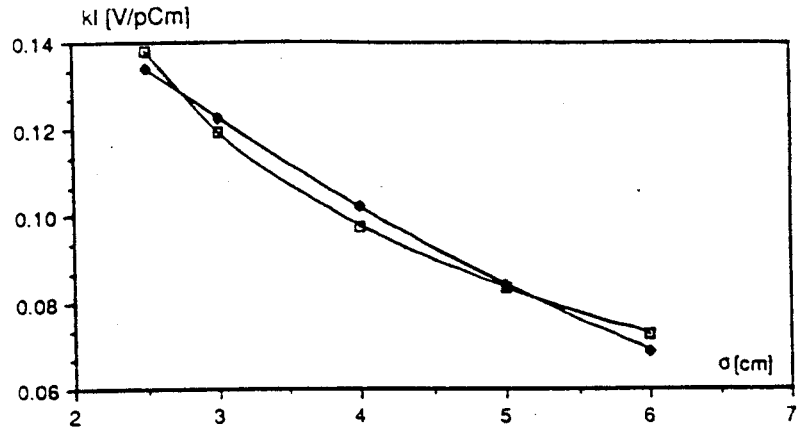

FIG. 6 – Dependence of the longitudinal loss factor on the bunch length for DAΦNE RF cavity; open squares: numerical results; full dots: broad–band resonator fit.

The model (1) with:

$$\frac{Z(n)}{n} = \left\{ -i\,0.0236 + \frac{18.76}{n} + \frac{263\,(1+i)}{n^{3/2}} \right\} \qquad (22)$$

where n is the harmonic number: $n = \omega/\omega_0$, gives much better results.

Figure 7 shows the fit of $k_l(\sigma)$, where the two curves, numerical and analytical, practically coincide. Also the fit of the wake–function is quite satisfactory for this model (see Fig. 8), while the wake–function, as given by the resonator model is rather different.

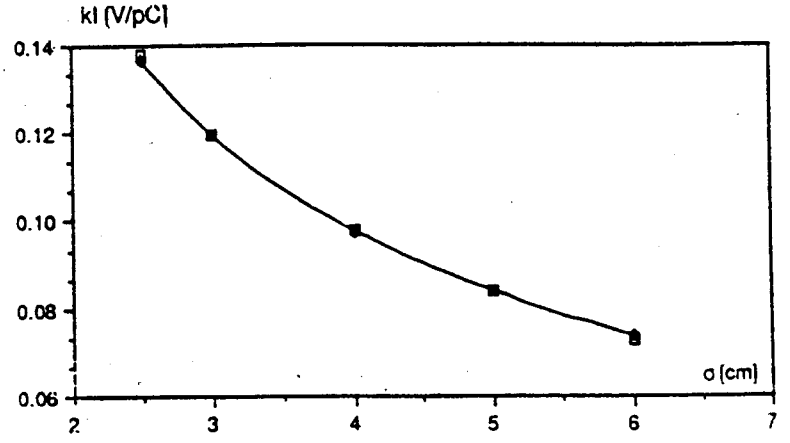

FIG. 7 – Fit of dependence $k_l(\sigma)$ with the broad–band model given by eq. (1).

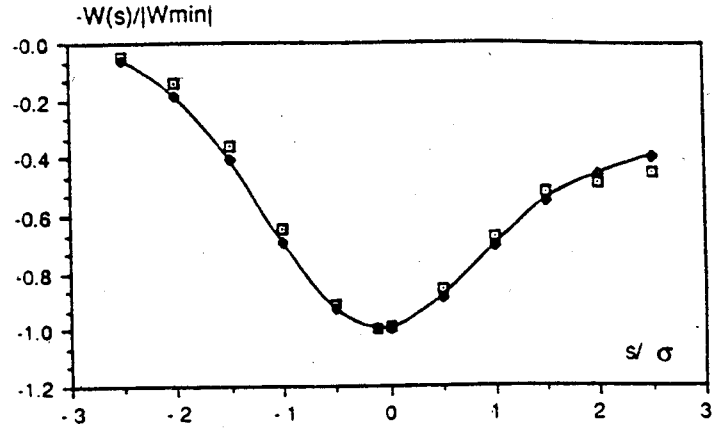

FIG. 8 – Fit of the normalized wake–function for DAΦNE RF cavity with the broad–band impedance model given by eq.(1).

Analytical and numerical curves coincide.

We could expect the impedance to behave like (22) since long tapers give mainly inductive contribution to the impedance and the cell with the large iris should behave like a pill–box cavity with attached tubes at high frequencies.

4. – INJECTION KICKER

Impedance estimate of the DAΦNE accumulator ring show that the main contribution to the longitudinal broad–band impedance comes from injection–extraction kickers, particularly from their tanks[9]. So, much attention is being paid now in the design of the injection kicker for the main rings.

It has been proposed to avoid any special tanks for the kickers and to put kicker's rods just inside the regular vacuum chamber with elliptic cross–section. The absence of the special tank is preferable also for multi–bunch operation, allowing to reduce the number of dangerous higher order modes and their impedance.

A 3D model of the kicker as used in simulations with MAFIA codes is shown in Fig. 9. In general, frequency behavior of the impedance depends on the loading conditions outside vacuum chamber (coaxial line, resistors, capacitances and so on). It is difficult to take into account these conditions with MAFIA. But we believe that the broad–band impedance does not depend very much on the load. According to the high frequency diffraction model[10] if a bunch does not "see" the surface, then this screened surface does not contribute to the broad–band impedance. So, if the load is somewhere outside and it is screened by other surfaces of the kicker it should not influence the broad–band impedance of the kicker, at least, at high frequencies.

It has been found that the first three terms of the expansion (1) describe well the broad–band impedance of the kicker:

$$\frac{Z}{n} = \left\{ -i\,0.083 + \frac{2.59}{n} + \frac{0.3722\,(1 - i)}{\sqrt{n}} \right\} \qquad (23)$$

Fits of the longitudinal loss factor (Fig. 10) and of wake–function (Fig. 11) confirm that.

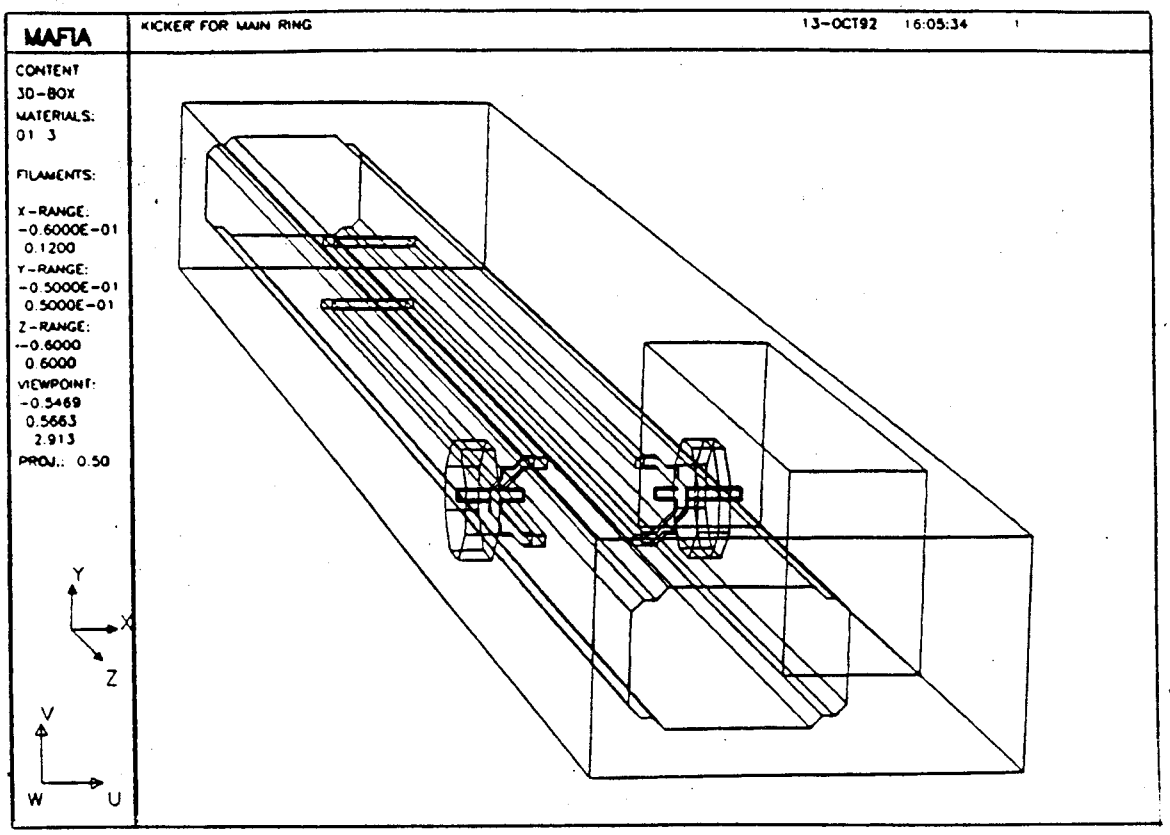

FIG. 9 – Injection kicker.

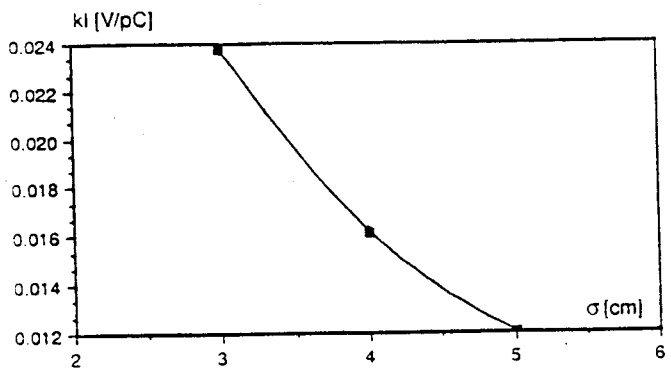

FIG. 10 – Fit of the longitudinal loss factor for the injection kicker; numerical and analytic curves coincide.

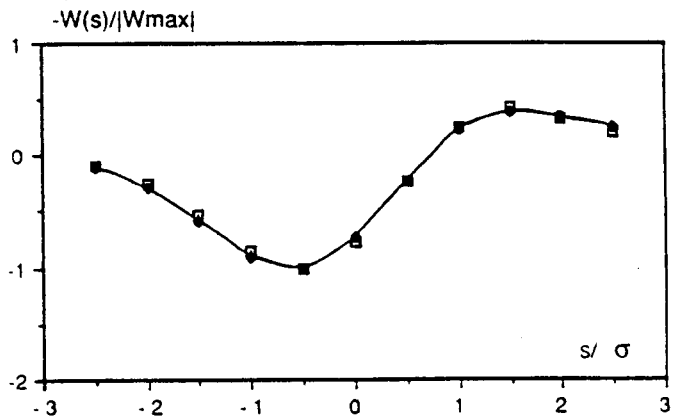

FIG. 11 – Fit of the normalized wake–function for the injection kicker; full dots: MAFIA code results; open squares: wake–function corresponding to the impedance model (1).

5. – LONGITUDINAL FEEDBACK KICKER

A longitudinal feedback system is necessary to damp the longitudinal multibunch instability[11]. The work on the system is now in progress. But just to understand how much a longitudinal feedback kicker could contribute to the broad–band impedance and whether the impedance model (1) is suitable for the kicker we take as an example the kicker proposed for ALS[12].

The 3D kicker model for MAFIA simulations is shown in Fig. 12. The wake–function for the kicker is presented in Fig. 13 and, as we can see, it corresponds to the third term in the impedance model (1). (For comparison see the wake–function in Fig. 3). The longitudinal loss factor scales as $\sigma^{-3/2}$ (Fig. 14) confirming this fact.

So, using the expression (17) we get for the kicker:

$$\frac{Z}{n} = \frac{1.51\,(1-i)}{n^{1/2}}\,\Omega \qquad (24)$$

We should mention here that the value of the loss factor is comparable with that of RF cavity. It suggests that the kicker cavity itself can be a source of Higher Order Modes (HOM) which are dangerous for multibunch operation.

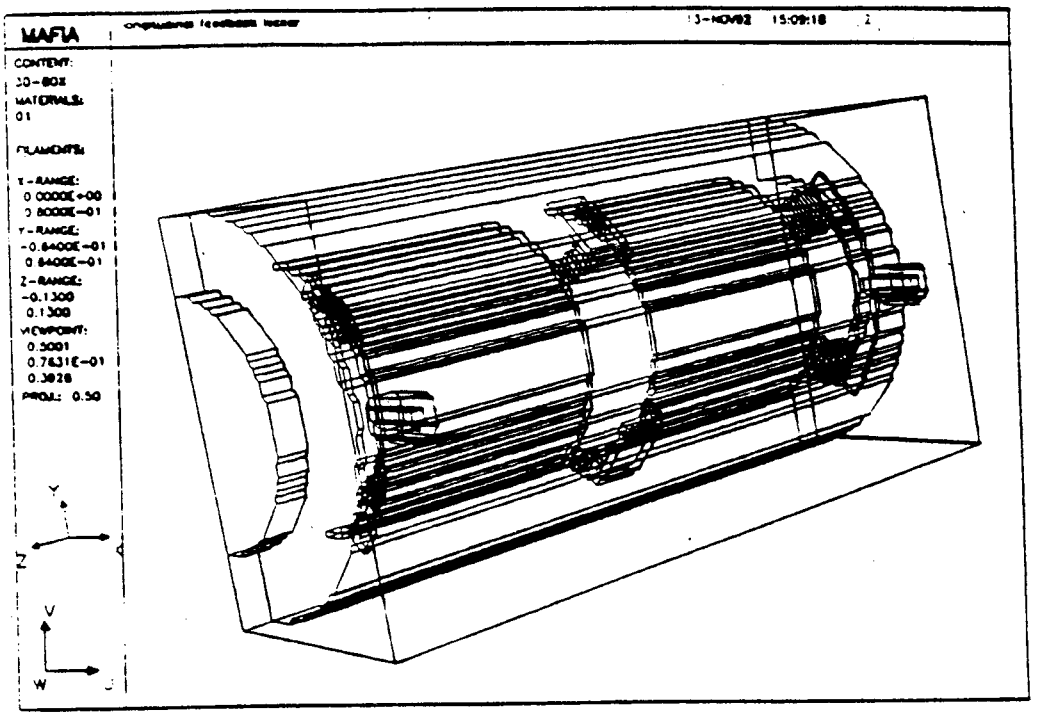

FIG. 12 – Longitudinal feedback kicker (half a structure).

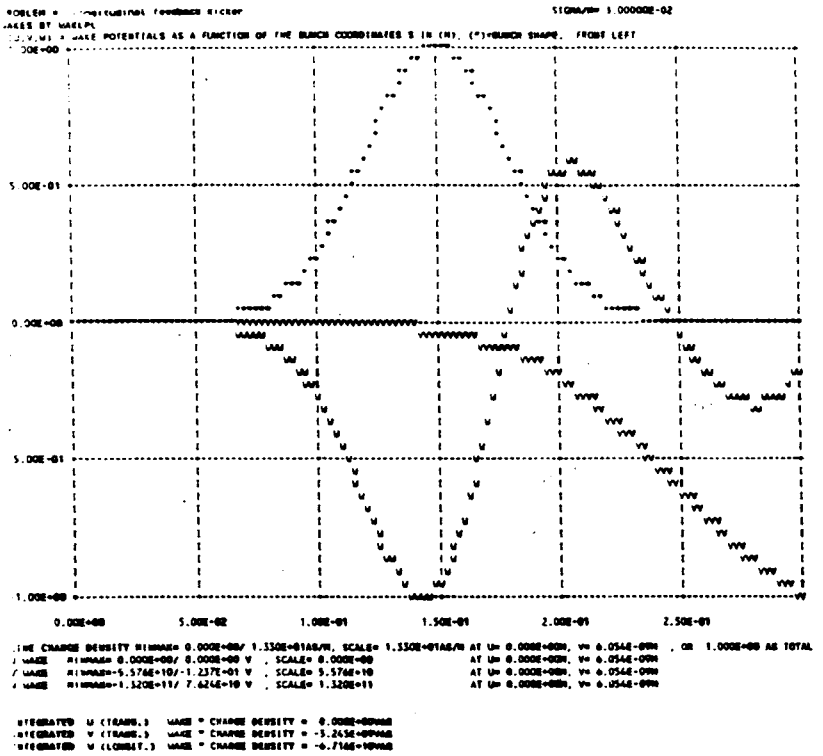

FIG. 13 – Normalized wake–function for the longitudinal feedback kicker (ω).

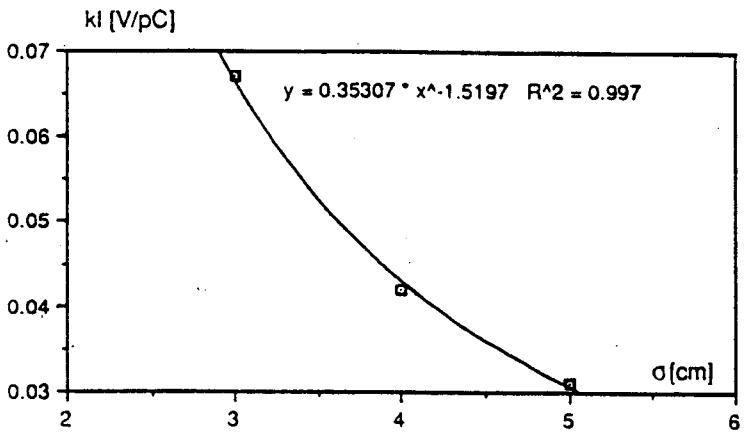

FIG. 14 – Dependence of the longitudinal loss factor on the bunch length for the longitudinal feedback kicker.

6. – INTERSECTION OF TWO RINGS

The intersection of two rings is another important impedance generating element. At this point two regular vacuum chamber merge in one common vacuum chamber of wider cross–section (Fig. 15).

Contribution to the impedance comes only from the part of the intersection where a bunch enters the wide vacuum chamber leaving the regular vacuum chamber.

A simple 3D model for MAFIA simulations is shown in Fig. 16. The part with the wide cross–section is rather long in order to simulate correctly the interaction between the bunch

and the synchronous harmonic of the electric field.

Fits of the wake–function (Fig. 17) and the longitudinal loss factor (Fig. 18) give for the structure:

$$\frac{Z}{n} = \frac{5.71\,(1+i)}{n^{3/2}} + \frac{0.096\,(1-i)}{n^{1/2}} \qquad (25)$$

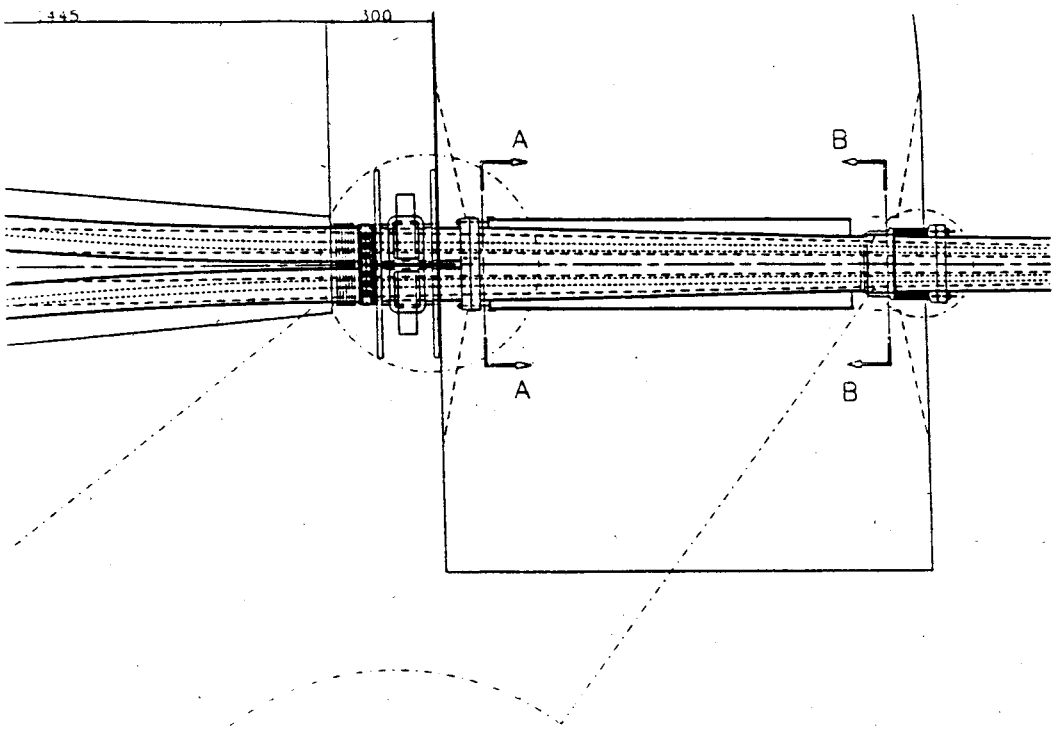

FIG. 15 – Intersection of two DAΦNE main rings.

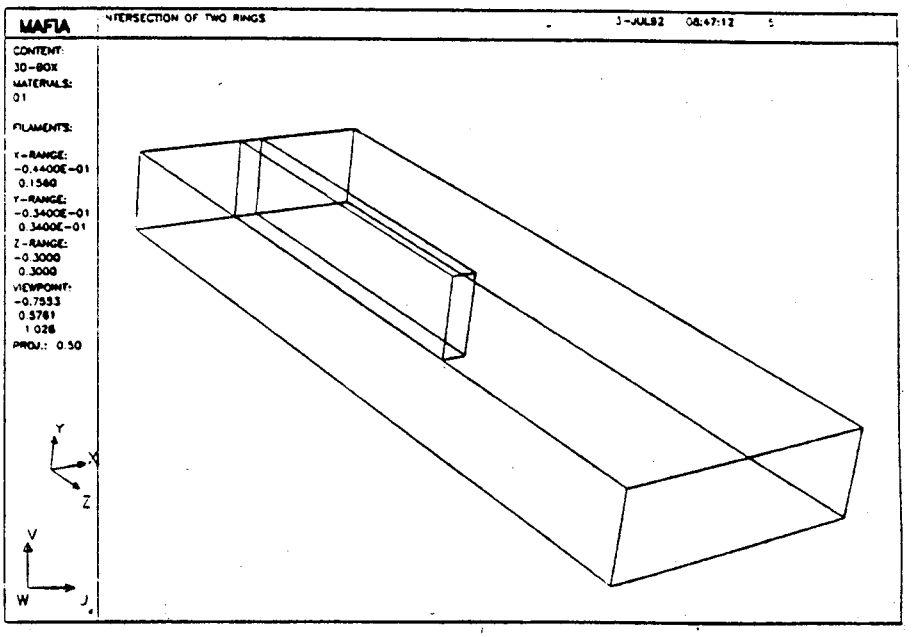

FIG. 16 – 3D model of the intersection of two rings.

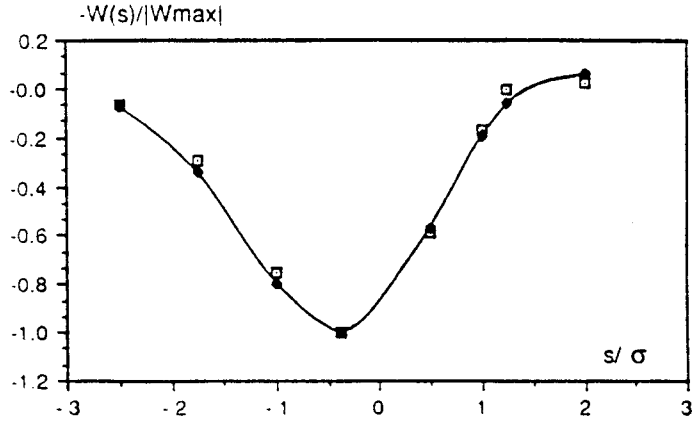

FIG. 17 – Fit of the normalized wake–function for the intersection of two rings; open squares: MAFIA code results; full dots: wake–function corresponding to the analytical impedance model (1).

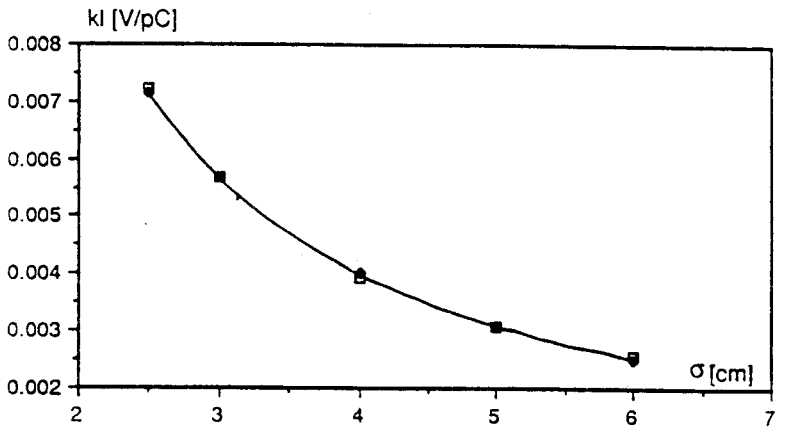

FIG. 18 – Dependence of the longitudinal loss factor on the bunch length. Numerical results (open squares) and analytic fit (full dots).

7. – SLOTS

A special antechamber is used in the main rings for pumping purposes and to install synchrotron radiation absorbers. The regular vacuum chamber and the antechamber are connected through slots. Figure 19 shows MAFIA code input which is used to simulate such kind of a structure.

There are 8 slots 2 cm wide and 120 cm long to accept synchrotron radiation in bending magnets and 4 slots 1 cm wide and 225 cm long in the vacuum chamber of wiggler magnets.

Numerical simulations show that in spite of the fact that the slots are relatively wide, the longitudinal loss factor is negligibly small and the wake–function is purely inductive for a bunch length of 3 cm. It is worth noting that the inductance of the slots practically does not depend on the slot length as soon as the length gets twice or three times longer than the width of the slots.

The formula (8) gives:

$$\frac{Z}{n} = -\,i\,8*10^{-5}\,\Omega \text{ per slot} \qquad (26)$$

for the slots in the bending magnets.

$$\frac{Z}{n} = -i\,8*10^{-5}\,\Omega \text{ per slot} \qquad (26)$$

for the slots in the bending magnets.

The vacuum chamber in the wiggler magnets has a vertical size (2 cm) much smaller than the horizontal one (13 cm). Because of such an asymmetry, effective image currents are concentrated on the upper and lower surfaces of the vacuum chamber in the vicinity of a bunch. The coupling between the bunch and the slots, situated far aside from that region, is very weak, giving negligible contribution to the impedance.

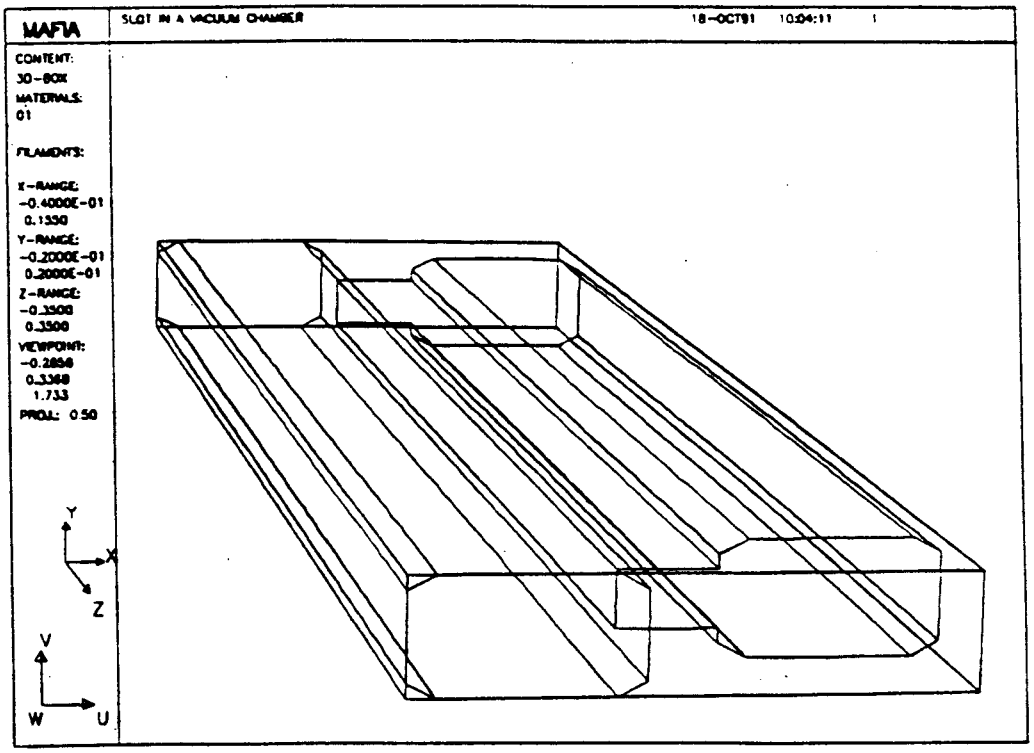

FIG. 19 – Slot between antechamber and regular vacuum chamber.

There are also four pumping ports in the interaction region (approximately 60 cm far from the interaction point) shielded with a perforated screen with 27 slots in each screen. One third of the screening surface is shown in Fig. 20 .

A single slot has an inductive impedance[13]:

$$Z(\omega) = -i\,Z_0 \frac{\omega}{c} \frac{(\alpha_e + \alpha_m)}{4\pi^2 b^2} \qquad (27)$$

where α_e and α_m are magnetic and electric polarizability, which can be calculated or measured.

For a rectangular slot of width w and length l, measurements in the range $0.2<l/w<1$ show the dependence[14]:

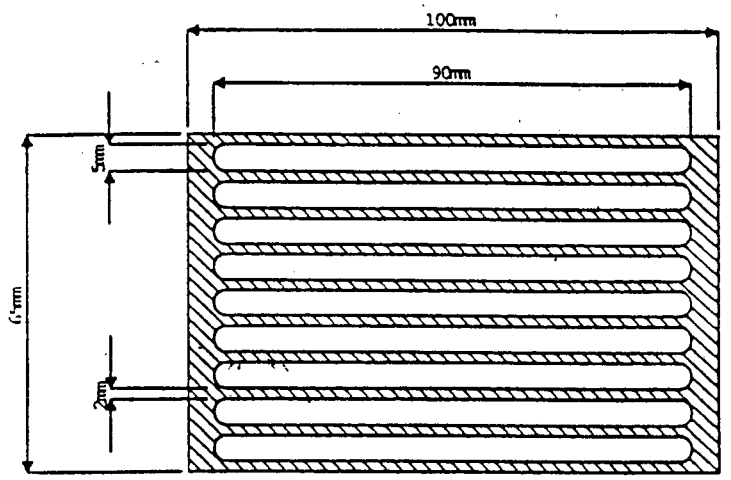

About 70 l/s each slot.
Total conductance: 550 l/s

FIG. 20 – Slots in the shield of the pumping ports.

Assuming the validity of the eq.(28) for our value of w/l = 0.056 we have

$$\alpha_e + \alpha_m = 0.048\, w^2 l \tag{29}$$

This gives for 4 pumping ports :

$$\frac{Z}{n} = -\,i\,5.48 * 10^{-3}\,\Omega \tag{30}$$

The estimate done for the elliptical slots with the same length and the effective width $w_{eff} = 4w/\pi$ gives a value which is approximately one order of magnitude smaller than that of eq. (30).

It is worth noting also that the coupling impedance falls down with wall thickness. For example, the coupling impedance of a circular hole reaches a value for an infinite thickness which is 56% of its value for zero thickness[15]. We should expect the same behavior also for slots.

Thus we have to consider the result (30) as an upper limit of the coupling impedance for the shielded vacuum ports.

8. – BELLOWS

Two different kinds of bellows will be used in DAΦNE main rings. The first one is similar to that used in PETRA and CESR. The convolutions of the bellows are shielded by sliding expansion joints (see Fig. 21). Bellows of that kind will be installed in straight sections.

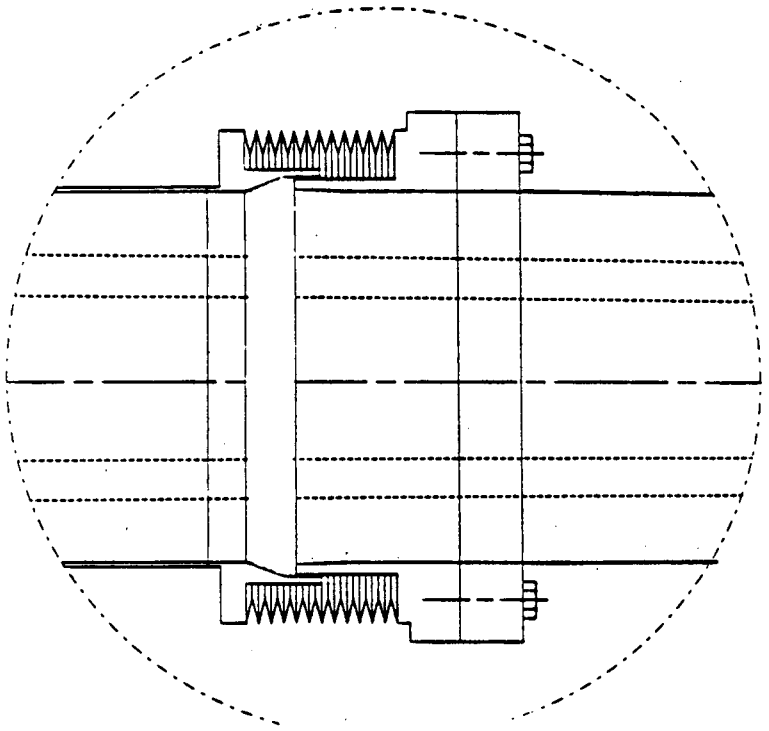

FIG. 21 – Bellows in the straight sections.

A shallow cavity, formed between the sliding joints gives purely inductive contribution to the impedance. TBCI gives for such a cavity:

$$\frac{Z}{n} = -i\,2.35*10^{-3}\,\Omega \qquad (31)$$

Bellows shielded by strips will be installed in the main ring arcs, allowing additional bending and rotation (see, for example, Ref. 16). Numerical data for the bellows are not available yet. But we believe that their coupling impedance is small and mainly inductive due to slots between shielding strips.

9. – TAPERS

In order to reduce the coupling impedance it is necessary to produce a vacuum chamber as smooth as possible. Very long tapers, connecting vacuum chamber components, are used in DAΦNE main rings to avoid sharp jumps in the vacuum chamber cross–section.

There are 8 such tapers, which are more than 1 m long, between a regular vacuum chamber in wiggler magnets (2 cm by 13 cm) and the regular vacuum chamber (4 cm by 9 cm). MAFIA code has some mesh size problems to simulate such a long and flat structure. To get an idea about the impedance we simulated the structure with TBCI replacing the rectangular cross–sections by circular ones[17]. As expected the wake–function is inductive, giving for the taper–in and the taper–out:

$$\frac{Z}{n} = -i\,5.5 * 10^{-3}\,\Omega \tag{32}$$

Two tapers are placed between the RF cavity beam pipes of 6 cm radius and the regular vacuum chamber. Their length is approximately 40 cm for both taper–in and taper–out and the contribution to the impedance is:

$$\frac{Z}{n} = \left\{ -i\,1.46 * 10^{-2} + \frac{0.075}{n} \right\} \Omega \tag{33}$$

Calculations have been done also with TBCI code for the structure consisting of the taper–in, the taper–out and a long straight circular pipe between these tapers.

There are tapers in the interaction region (see Fig. 22). The cavity near the interaction points is shielded by a thin beryllium layer, having the same radius as attached beam tubes. In this case only two tapers on both sides of the interaction point will contribute to the impedance. Analysis of the wake–function given for the azimuthally symmetric structure by TBCI gives the impedance:

$$\frac{Z}{n} = \left\{ -i\,0.011 + \frac{0.11}{n} \right\} \Omega \tag{34}$$

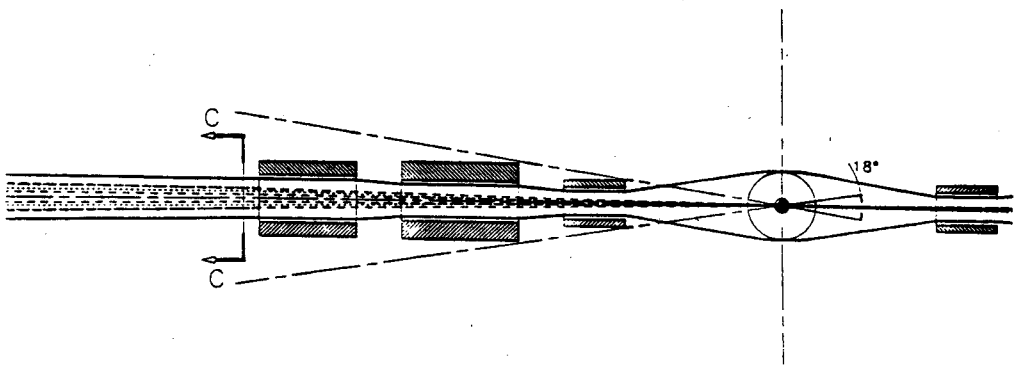

FIG. 22 – Tapers in the Interaction Region.

10. – RESISTIVE WALL IMPEDANCE

Most part of the main ring vacuum chamber has almost rectangular cross–section with rounded corners. For a rectangular beam pipe the resistive wall impedance per unit length is given by[18]:

$$\frac{Z(\omega)}{L} = Z_0 \frac{\omega}{2\pi c} \frac{(1-i)\,\delta}{2b} F_0\left(\frac{b}{a}\right) \tag{35}$$

where 2a and 2b are the horizontal and vertical sizes of the beam pipe. The coefficient F_0 is equal to:

$$F_0(\lambda) = \pi \left[\sum_{n=1\,(odd)}^{\infty} \frac{1}{\cosh^2(n\pi/2\lambda)} + \lambda \sum_{n=1\,(odd)}^{\infty} \frac{1}{\cosh^2(n\pi\lambda/2)} \right] \qquad (36)$$

DAΦNE vacuum chamber has sizes 2a = 9 cm and 2b = 4 cm. F_0 at these values of a and b is very close to 1. So for the vacuum chamber made of aluminum eq. (35) gives for the ring total resistive wall impedance:

$$Z(\omega) = 10^{-4}(1 - i)\sqrt{\omega} \qquad (37)$$

and the normalized value:

$$\frac{Z}{n} = \frac{0.44(1 - i)}{\sqrt{n}} \qquad (38)$$

11. – CONCLUSIONS

The broad–band longitudinal impedance of DAΦNE main ring vacuum chamber components we have considered is described reasonable well by four terms of the expansion (1).

Total impedance over these elements is:

$$\frac{Z}{n} = \left\{ -i\,0.26 + \frac{24.8}{n} + \frac{(1 - i)\,2.89}{n^{1/2}} + \frac{(1 + i)\,274.42}{n^{3/2}} \right\} \Omega \qquad (39)$$

Figure 23 shows the imaginary and the real part of the normalized impedance as a function of the harmonic number n with superimposed bunch spectrum.

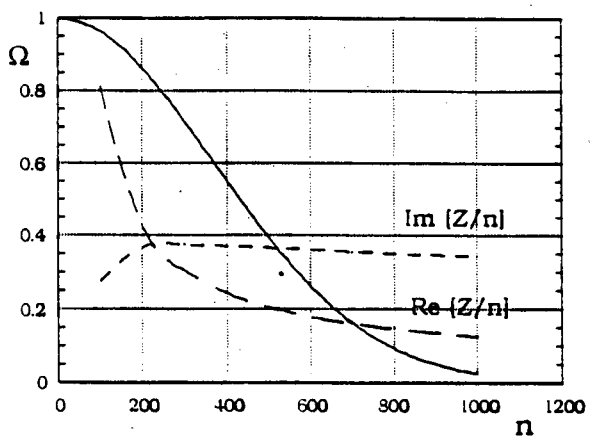

FIG. 23 – Imaginary and real part of DAΦNE main ring impedance with superimposed bunch spectrum (solid line).

We realize that not all impedance generating elements are included in eq. (39). Other tapers, flanges, slots etc. can be included during further development of the vacuum chamber design. We believe that the impedance of the elements is mainly inductive and the careful design will help to keep the effective broad–band impedance within 1 Ω which is the design limit.

REFERENCES

1. A. Hofmann, J. Maidment, "Current dependent phenomena in LEP", CERN LEP note 168 (1979).
2. K. Bane, "The Calculated Longitudinal Impedance of the SLC Damping Ring", SLAC–PUB–4618 (1988).
3. S. Heifets, "Broad Band Impedance of the B–factory", SLAC/AP–93, February 1992 (AP).
4. T. Weiland, "Transverse Beam Cavity Interaction, Part. I: Short Range forces", Nucl. Instrum. Methods 212 (1983), p.13.
5. R. Klatt and T. Weiland, "Wake field calculations with three–dimensional BCI code", ldProceedings of Linear Accelerator Conference, SLAC, (1986), p.282.
6 I. S. Gradshteyn and I. M. Ryzhik, "Tables of Integrals, Series, and Products", fourth edition.
7. A. Piwinski, "Wake–fields and Ohmic Losses in Round Vacuum Chambers", DESY HERA 92–11, May 1992.
8. DAΦNE Machine Project, "Contributions to the 3rd European Particle Accelerators Conference (EPAC 92)", LNF–92/033 (P), Aprile 1992.
9. "Impedance budget and RF Losses", presented by M. Zobov at 3 DAΦNE Review, 7–9 July 1992.
10. S. Heifets, "Diffractive Model of the High Frequency Impedance", Physical Review D, V. 40, No. 9, p.3097.
11. L. Palumbo, "Coupled Bunches Instabilities in DAΦNE", DAΦNE Technical Note G–10, Dec. 18 1991.
12. F. Voelker and J. Johnson, "Status of RF Feedback Kicker Design", Asymmetric B–factory Collider Note, ABC–69,April 27 1992.
13. S. S. Kurennoy, "Beam Coupling Impedance of Holes in Vacuum Chamber Walls", IHEP Preprint 92–84, Protvino 1992.
14. R. L. Gluckstern , R. Li and R.K. Cooper, "Corrections to Electric Polarizability and Magnetic Susceptibility of Small Holes in a Thin Screen", IEEE Trans. on Microwave Theory and Techniques, 1990, V. 38, p. 1529.
15. R. L. Gluckstern, "Coupling Impedance of a Single Hole in a Thick Wall Beam Pipe", CERN SL/92–05 (AP), January 1992.
16. S. Be, "Design of Vacuum Chamber Components Including Step Changes for the 6–GeV Storage Ring", in Proceedings of Workshop "Impedance and Current Limitation", October 17–18 1988, Grenoble.
17. L. Palumbo, V. G. Vaccaro, G. Wustefeld, "Coupling impedance in a circular Particle Accelerator, a Particular case: Circular beam, Elliptic Chamber", IEEE Trans. on Nucl. Science, V. NS–31, No. 4,p.1011.
18. R. L. Gluckstern, J. van Zeijts, B. Zotter, "Coupling Impedance of Beam Pipes of General Cross Section", CERN SL/AP 92–25, June 1992.